JTTEE5 8:102-109

Thermal Diffusivity/Microstructure Relationship in Y-PSZ Thermal Barrier Coatings

F. Cernuschi, P. Bianchi, M. Leoni, and P. Scardi

(Submitted 2 June 1998; in revised form 20 December 1998)

A set of yttria partially stabilized zirconia coatings with different thickness was deposited on flat nickel-base alloy coupons by air plasma spray (APS) under uncontrolled temperature conditions. In this way, the length of the spraying process (and consequently the coating thickness) had a direct effect on phase composition as well as on the thermal properties of the material. In particular, both the monoclinic phase percentage and thermal diffusivity increased considerably with the thickness. Because this trend was observed together with a slight but clearly visible increase in the total porosity, the interpretation of the results was not straightforward, but required a detailed discussion of the thermal transport mechanism. Considering the complex microstructure typical of APS coatings and the relevant role of porosity, it was shown how a modest reduction in the fraction of closed pores can account for the observed increase in diffusivity. It was then proposed that the volume change associated with the progressive tetragonal to monoclinic phase transformation can be responsible for the reduction of the closed porosity of lenticular shape oriented parallel to the surface, in spite of the observed increase in the total porosity.

Keywords air plasma spray, photothermal radiometry, thermal barrier coatings, thermal diffusivity, XRD, Y-PSZ

1. Introduction

Thermal barrier coatings (TBCs) find an increasing number of applications to protect high-temperature metallic components; for example, TBCs are deposited on transition pieces, combustion liners, first-stage vanes, and other hot-path components of gas turbines either to increase the inlet temperature with a consequent improvement of the efficiency or to reduce the requirement for a cooling system (Ref 1-3).

To be effective, TBCs should satisfy various requirements:

- To have a thermal diffusivity as low as possible
- Should not exhibit any phase transition during thermal cycling (which is the typical thermal solicitation in combustion engines)
- To be strongly adherent to the substrate
- To hinder the oxidation and corrosion phenomena of both metallic bondcoat and substrate.

The best compromise among these different requirements is presently offered by partially stabilized zirconia, such as 7 to 8 wt% Y_2O_3-ZrO_2 (Y-PSZ), deposited either by the air plasma spray (APS) technique or by electron beam physical vapor deposition (EB-PVD). As far as APS is concerned, great attention must be paid to process parameters such as substrate temperature, powder size, deposition atmosphere, and so forth (Ref 4), which affect the final TBC microstructure.

Thermal diffusivity in plasma sprayed coatings depends on grain size, morphology, porosity, and phase composition; therefore its evaluation is essential to assess the effectiveness of TBCs. Several techniques can be used for thermal diffusivity measurements. The laser flash method is a worldwide applied technique, but samples with precisely defined dimensions are required. Because it is not always possible to extract samples from coated components, some nondestructive techniques directly applicable to coated components have been developed. In particular, photothermal techniques, such as time-resolved infrared radiometry (TRIR) and thermal wave interferometry (TWI), can be used for measuring thermal diffusivity of TBC deposited on samples of any size, provided that they are wider than the heating spot of the used laser beam (Ref 5-7).

In this work, the authors investigated thermal diffusivity, phase composition, and porosity for a set of Y-PSZ coatings deposited on flat nickel-base alloy substrates by APS. Possible correlation among these parameters, coating thickness, and spraying conditions is discussed.

2. Photothermal Technique: Theoretical Remarks

Time-resolved infrared radiometry allows the measurement of both coating thickness and thermal diffusivity, as well as the detection of delamination on multilayered samples. This is done by time-resolved measurement of surface temperature changes induced by the application of a step heating supplied by a cw laser source.

The time evolution of surface temperature for a two-layer sample heated uniformly on its surface depends both on coating thickness, L, and on thermal diffusivity, $\alpha = k/\rho C$, as follows (Ref 5):

F. Cernuschi and **P. Bianchi,** ENEL Struttura Ricerca, Polo Diagnostica e Materiali, via Rubattino 54, 20134 Milano, Italy; and **M. Leoni** and **P. Scardi,** Dipartimento di Ingegneria dei Materiali, Università di Trento, 38050 Mesiano (TN), Italy. Contact e-mail: Paolo.Scardi@ing.unitn.it.

$$T(t) = \frac{2Q}{\varepsilon_1\sqrt{\pi}}\sqrt{t}\cdot\left[\frac{1}{\sqrt{\pi}} + 2\sum_{n=1}^{\infty} R^n\left\{e^{-n^2L^2/\alpha_1 t} - \frac{nL}{\sqrt{\alpha_1 t}}\left[1 - \mathrm{erf}\left(\frac{nL}{\sqrt{\alpha_1 t}}\right)\right]\right\}\right] \quad \text{(Eq 1)}$$

where ρ, C, k, and Q are density, thermal capacity, thermal conductivity, and power density, respectively; $\varepsilon = \sqrt{\rho C k}$ is the thermal effusivity, and R is the heat reflection coefficient, defined as:

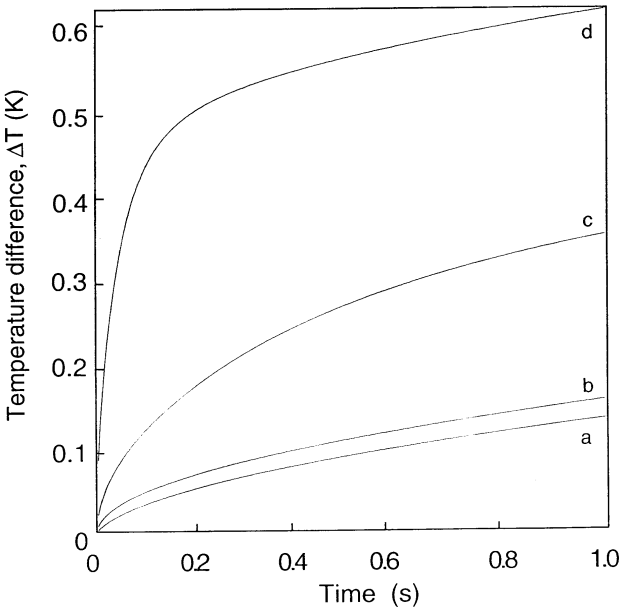

Fig. 1 Surface temperature change (ΔT) as a function of time, according to Eq 1, calculated for four different coating materials deposited on a Nimonic 90 substrate. (a) Plasma sprayed Al_2O_3 ($\alpha = 0.85 \times 10^{-6}$ m^2/s and $\varepsilon = 700$ J/m^{2}Ks$^{1/2}$). (b) Plasma sprayed YPSZ ($\alpha = 0.1 \times 10^{-6}$ m^2/s and $\varepsilon = 2800$ J/m^{2}Ks$^{1/2}$, Ref 8). (c) Nimonic 90 ($\alpha = 3 \times 10^{-6}$ m^2/s and $\varepsilon = 7000$ J/m^{2}Ks$^{1/2}$). (d) Pure iron ($\alpha = 20 \times 10^{-6}$ m^2/s and $\varepsilon = 17{,}000$ J/m^{2}Ks$^{1/2}$, Ref 6). Coating thickness and heating conditions were the same in all cases: 300 μm and 1000 W/m^2, for thickness and power density, respectively.

$$R = \frac{\varepsilon_1 - \varepsilon_2}{\varepsilon_1 + \varepsilon_2} \quad \text{(Eq 2)}$$

where the subscripts 1 and 2 refer to coating and substrate, respectively. The summation over n takes into account multiple reverberations of the heat pulse between the interfaces. If either L or α is known, from Eq 1 it is thus possible to determine both L^2/α and R by a nonlinear regression technique.

As an example, Fig. 1 shows several curves calculated by Eq 1 for a constant coating thickness of 300 μm and different thermal diffusivity values.

3. Experimental

3.1 Materials

Substrates were flat rectangular plates (2 by 3 cm^2) of Nimonic 90 (Inco, USA), a nickel-base alloy whose composition and thermophysical properties are reported in Table 1. Several coated samples with different thickness were deposited by APS from a Starck Amperit 825.0 (H.C. Starck, Germany) (ZrO_2 + 7wt%Y_2O_3) powder, following manufacturer instructions (Metco 9MB gun, procedure No. 4, Ref 9).

Zirconia is a translucent material; that is, visible light is not absorbed by the surface in the first tens of nanometers (as in metals), but it can be scattered and transmitted to depths of some millimeters. Because the adopted TRIR model (see section 2) requires light to be converted into heat on the sample surface, it is incompatible with the translucent behavior. Therefore, in order to limit the penetration of light inside the sample, a thin gold layer (less than 50 nm) was sputtered on the sample surface.

3.2 TRIR Experimental Setup

Figure 2 shows the experimental setup: the heating source is a 5 W Ar ion laser (Spectra Physics 2020, Spectra Physics Lasers, Inc., Mountain View, CA). In order to obtain a square wave, the laser beam is intercepted by an electronic shutter (846HP, Newport digital shutter; Newport Co., USA). A beam splitter after the shutter deflects a portion of the beam toward a photodiode

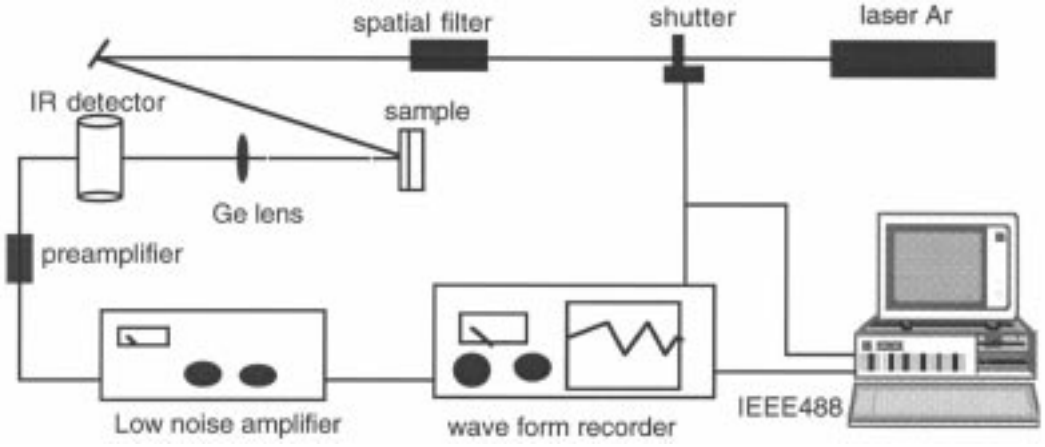

Fig. 2 TRIR experimental setup (see text)

to generate a trigger signal for the infrared data acquisition detector. A spatial filter allows the laser beam size to be varied on the heated sample.

The surface temperature of the sample during heating was monitored by an infrared detector (EG&G Judson J15D12, EG&G Judson, Montgomeryville, PA), and the signal (amplified by a low-noise SR530 device, Stanford Research Systems, SRS, Sunnyvale, CA) was collected by a waveform recorder (Data 6100, Data Precision, division of Analogic Co., USA). Each instrument was controlled by a personal computer, which also computed coating thermal diffusivity from the experimental data.

3.3 X-Ray Diffraction Measurements

A Rigaku PMG-VH x-ray diffractometer (Rigaku Co., Japan) was used for data collection of patterns in the Bragg-Brentano geometry. The instrument, equipped with suitably narrow slits and a graphite bent crystal analyzer in the diffracted beam, gives narrow and symmetrical instrumental profiles, even in the angular region encompassed by the low-indices peaks of Y-PSZ polymorphs (above $2\theta \approx 25°$). Under these conditions, the instrumental resolution function (IRF) could be carefully measured by means of a profile standard KCl powder (Ref 10). The IRF, in parametric form, as obtained by profile modeling, was then embodied in a whole powder pattern fitting (WPPF) numerical program based on the Rietveld method, which was used for a standardless quantitative phase analysis. Details on the procedure can be found elsewhere (Ref 11).

3.4 Optical Microscopy

Thickness measurements were performed by optical microscopy on cross-sectioned samples after metallographic polishing, and the values are reported in Table 2. The same samples were used to estimate the porosity level within the ceramic coating by image analysis. A Leica Q500MC (Leica Microsystems, Cambridge, UK) video image analyzer was used, and an average of more than 30 measurements on different spots is reported. To improve the image contrast, a thin gold layer was deposited on the samples prior to the observation.

4. Results

Figure 3 shows a portion of the XRD pattern of three coatings with different thickness: 11 μm (A1), 207 μm (A5), and 321 μm (A8). Even without a detailed analytical evaluation, it is apparent that:

- A1 is sufficiently thin that the x-ray beam penetrates to the superalloy substrate, whose (111) peak (identified as Nim. 90) is visible in the pattern.
- The monoclinic phase percentage increases with the thickness.
- A residual percentage of yttria is present (see the inset of Fig. 3).

It must be considered that sample A1 (the only one whose thickness is such to give a diffracted signal from the substrate) is not a homogeneous mixture of crystalline phases, but displays a layered structure, made of a two-phase coating (tetragonal (t) and monoclinic (m) zirconia) and a single-phase (fcc) metal substrate. In order to account for these features, the program Xmas was employed. Based on the Rietveld refinement method, the program allows standardless phase analysis both for homogeneous phase mixtures (powder samples) and for layer structure as of interest for sample A1. In the last case, an effective layer thickness can be refined together with the traditional structural parameters (Ref 11). Figure 4 shows the results for sample A1: both experimental (dot) and calculated (line) patterns are displayed together with their difference (the upper "residual" line). The corresponding effective thickness was estimated to be 8.3(1) μm ("effective" indicates that porosity does not contribute to this determination, and the presented value is that of a corresponding 100% dense layer). By comparing the effective thickness with the optically measured one, an average porosity of ~24% can be calculated.

This procedure was used for the other samples, where the conventional model of a homogeneous phase mixture was appropriate. The results are reported in Fig. 5, where phase percentages are plotted against coating thickness. The linear correlation between zirconia polymorph percentages and thickness is apparent. The yttria phase content is roughly a constant for all the coatings but A1, where no yttria phase was found.

Table 1 Nimonic 90 thermophysical properties and chemical composition

Density, kg/m^3	Specific heat, J/kg · K	Thermal conductivity, W/m · K	Thermal diffusivity, m^2/s	Thermal effusivity, J/Km^{2}s$^{1/2}$
8180	446	11.4	0.031×10^{-4}	6468

Chemical composition, wt %													
C	Si	Cu	Fe	Mn	Cr	Ti	Al	Co	B	S	Pb	Zr	Ni
<0.13	1	0.2	1.5	1	18-21	2-3	1-2	15-21	<0.02	<0.015	<0.002	<0.15	bal

Table 2 Coating thickness and thermal diffusivity data

	Sample							
	A1	A2	A3	A4	A5	A6	A7	A8
Optical thickness, μm	11 ± 6	63 ± 11	84 ± 12	117 ± 13	207 ± 14	224 ± 8	267 ± 13	321 ± 13
Diffusivity × 10^{-3}, cm^2/s	…	1.7	1.9	1.8	2.6	2.3	2.9	2.7

The only significant difference in line profiles was observed between sample A1 and all the others. The 11 μm coating displayed broader profiles because the size of coherent diffraction domains and microstrain due to lattice defects were, respectively, smaller and higher than in the other, thicker samples.

The microstructure of the coating was typical of plasma sprayed ceramic TBCs, with lamellar grains and a complex pattern of cracks and voids. The only relevant difference with thickness was the development of large longitudinal cracks for thickness above ~100 μm. This feature can be appreciated in Fig. 6, where the optical micrographs of A3 and A6 are shown. As described in the previous section, image analysis was employed to estimate the porosity level within the ceramic coatings, and to this purpose the void area was measured on several spots for each cross-sectioned sample. It can be noted that this procedure can be affected by errors arising from the sample preparation. In addition, optical microscopy does not allow observation of small pores and cracks; therefore, only average values could be obtained with the purpose of comparing samples of the same series.

A reasonable estimate of the total porosity was obtained from sample A9, whose coating spontaneously detached from the substrate, so that the density could be calculated from a direct measurement of weight and volume. The measured value was 4.39 g/cm^3, which considering a theoretical density of 5.95 g/cm^3 (as obtained from XRD, taking into account the actual phase composition), gives an average porosity of 26.2%. In this way, it was possible to normalize the void area percentages and calculate the equivalent porosity for all samples (Fig. 7). Even taking into account the estimated error, the porosity level, on average, slowly increases with thickness.

Thermal diffusivity measurements for samples A2 and A5 (Fig. 8) indicate good agreement between experimental and modeled data (the trend for the other samples was qualitatively similar). These modeled data were obtained from the best fit of

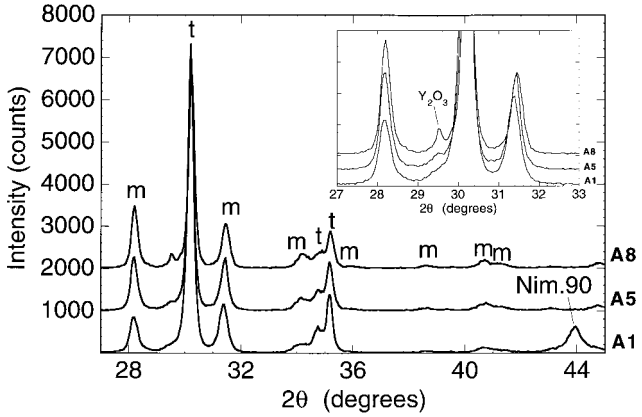

Fig. 3 Low-angle portion of the XRD pattern of samples A1 (a), A5 (b), and A8 (c). Peaks belonging to tetragonal (t), monoclinic (m), yttria (Y_2O_3), and Nimonic 90 (Nim.90) substrate are reported.

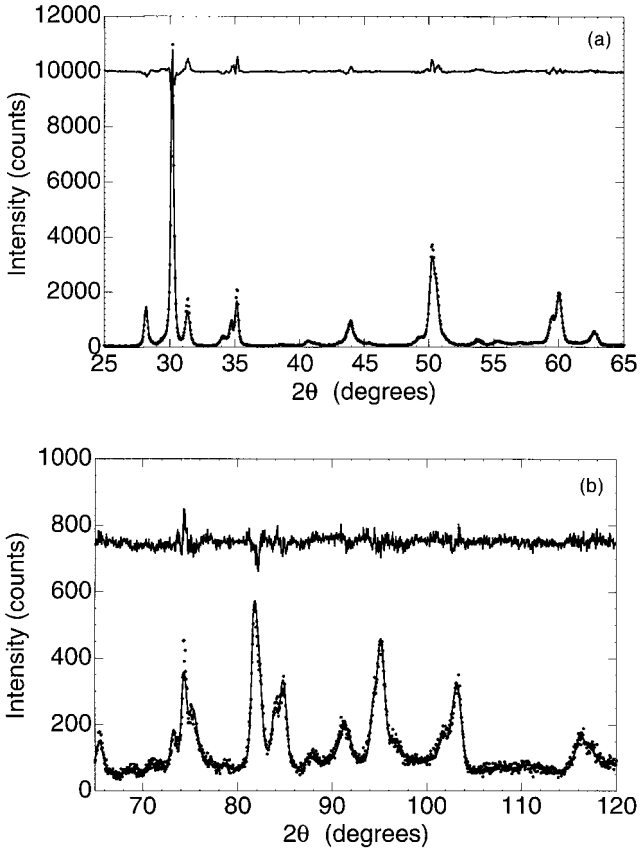

Fig. 4 Graphical output of WPPF for sample A1, showing low-angle (a) and high-angle (b) ranges. Experimental (dot) and modeled (line) data are reported together with their difference (residual), above.

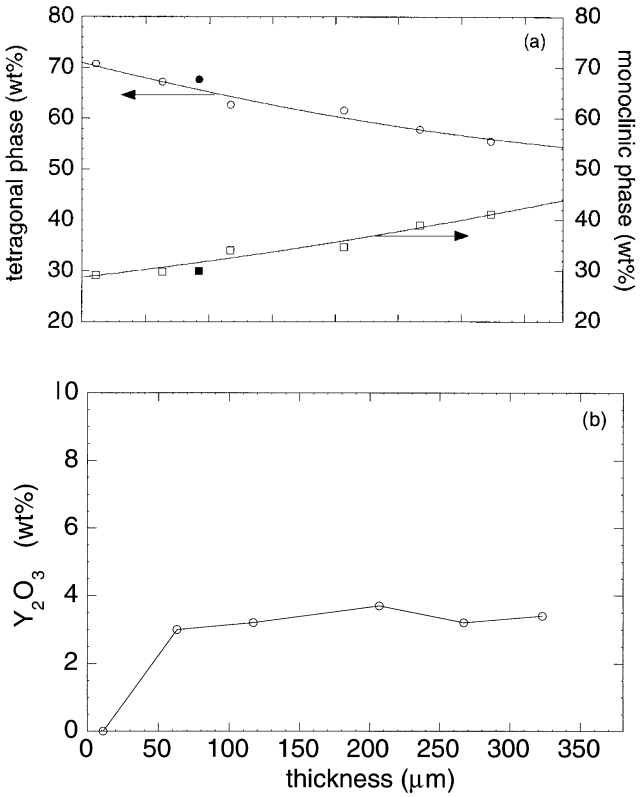

Fig. 5 Phase composition, as obtained from the WPPF procedure, as a function of coating thickness. Zirconia polymorphs (a) and Y_2O_3 (b) content

Eq 1, keeping the coating thickness and substrate thermal parameters constant during the numerical procedure. In this way, a best fit value of L^2/α was obtained, from which thermal diffusivity could be calculated by using the thickness values optically measured on cross-sectioned samples. Sample A1 was not sufficiently thick to be reliably measured.

Figure 9 shows a possible correlation between thermal diffusivity and coating thickness. Moreover, from the comparison of TRIR and XRD results, a further relationship can be established between thermal diffusivity and t/m phase composition. Its nature is discussed in the next section.

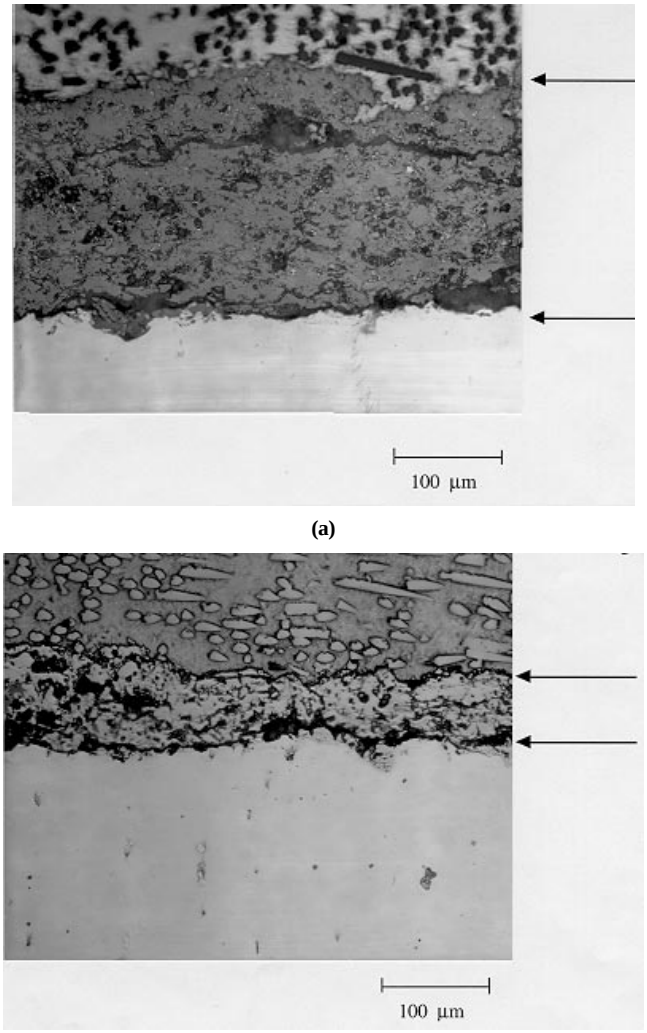

Fig. 6 Optical micrographs (200×) of cross-sectioned samples A3 (a) and A6 (b). Arrows mark the ceramic coating.

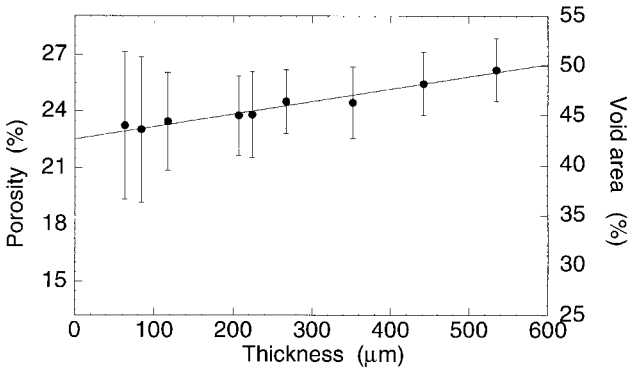

Fig. 7 Average porosity (left axis) and empty area (right axis) percentage versus coating thickness. The solid line is the linear regression of the experimental data.

5. Discussion

The dependence of phase composition with thickness, as obtained by WPPF of XRD patterns, can be interpreted by considering the spraying conditions. Coatings are deposited on metallic substrates by a multiple-pass process, so the longer the spraying time, the thicker the coating. If sample temperature during the deposition is not controlled, and consequently no specific cooling of the coated surface is realized, a close correlation between coating thickness (i.e., spraying time) and surface temperature of the coating can be expected.

Due to the low thermal conductivity of the ceramic, only the A1 coating, whose thickness roughly corresponds to a single pass of the plasma torch, exhibits good thermal exchange with the metal substrate. For the other samples, the coating temperature increased with the thickness, leading to a progressive destabilization of the material. In fact, it is known that plasma sprayed zirconia coatings are highly metastable and their phase evolution depends on the spraying parameters as well as on the subsequent service conditions. The development of large longitudinal cracks can also be associated with this feature, keeping in mind that large cracks such as those observed on sample A6 in Fig. 6 could be partially due to the preparation of the cross section.

To discuss the observed relations among microstructure, phase composition, and the property of interest to the present work, that is, thermal diffusivity, it is necessary to consider the effect of shape and percentage of porosity on the heat conduction mechanism. Among those present in the literature, a model in which the pores are ellipsoid-shaped (Ref 12-15) can be used

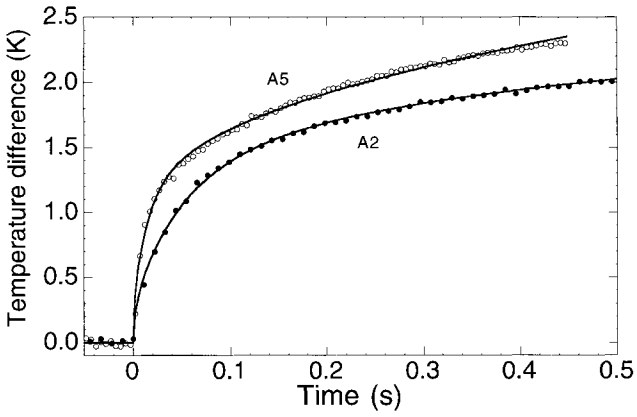

Fig. 8 Experimentally measured surface temperature versus time for samples A2 (solid circle) and A5 (open circle). The starting temperature (i.e., at shutter opening) is set to zero by subtracting a baseline recorded before heating. The solid curves in both figures were calculated by the model of Eq 1.

to describe the influence of porosity on thermal conductivity, k. In particular, this influence can be represented by the following equation (Ref 12, 13):

$$k/k_0 = (1-p)^x \quad \text{(Eq 3)}$$

where k_0 and p are the bulk thermal conductivity and the porosity percentage, respectively:

$$x = \frac{1-\cos^2\vartheta}{1-F} + \frac{\cos^2\vartheta}{2F} \quad \text{(Eq 4)}$$

where ϑ is the angle between the thermal flux and the axis of revolution, and F is the shape factor of the ellipsoid. In Fig. 10, Eq 3 is plotted for different porosity shapes. The only reliable description for the open porosity is that given in terms of cylindrical pores (Ref 12); an equivalent model can be formulated, leading to the expression (Ref 12):

$$(1-p)(k_0-k)\left[\frac{2(1-\cos^2\vartheta)}{k_0+k} + \frac{\cos^2\vartheta}{k}\right] = P(2-\cos^2\vartheta) \quad \text{(Eq 5)}$$

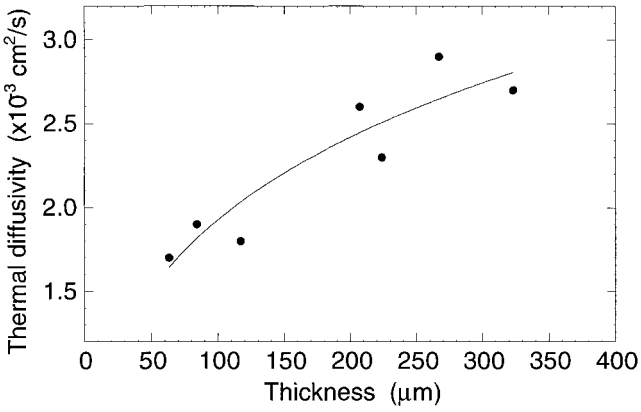

Fig. 9 Thermal diffusivity as a function of coating thickness.

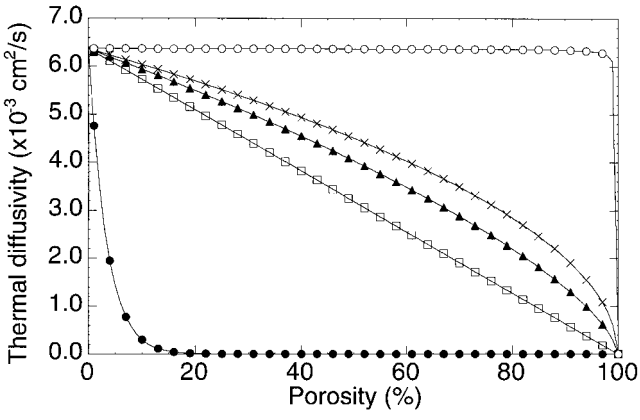

Fig. 11 Thermal diffusivity versus porosity for ●, lamellas, □,cylinders perpendicular to the thermal flux; ▲, cylinders randomly oriented; ×, spheres, and ○, lamellas and cylinders parallel to the thermal flux. Computation was performed using the following bulk data: ρ = 5.8 g/cm^3, C = 460 J/g · K, k = 1.7 W/m· K.

that, in the approximation of random porosity, simplifies as:

$$k/k_0 = \left[\left(\frac{4-9p}{10}\right) + \sqrt{\left(\frac{4-9p}{10}\right)^2 + \frac{1-p}{5}}\right] \quad \text{(Eq 6)}$$

The results do not differ from the curve for randomly oriented cylinders in Fig. 10. It is evident that the higher the porosity, the lower the thermal conductivity. The effect of porosity on thermal diffusivity can be evaluated by finding the dependence of both density and specific heat on the porosity itself.

As expected, Fig. 11 shows that the thermal diffusivity also decreases by increasing porosity. Most importantly, it is observed that lamellar porosity perpendicular to the flux has a dramatic effect on diffusivity; however, any variation above ~10% produces only negligible changes. On the contrary, when cylinders are considered (both random and oriented), the porosity variation produces an almost constant change in the thermal diffusivity.

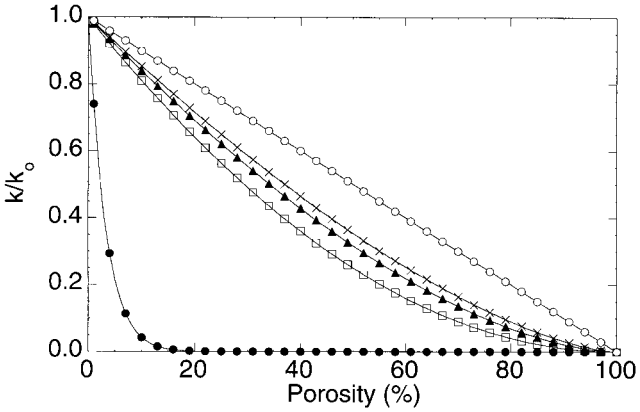

Fig. 10 Normalized thermal conductivity (k/k_0) versus porosity for different porosity geometry. ●, lamellas and □, cylinders, perpendicular to the thermal flux;▲, randomly oriented cylinders; × spheres, and ○, lamellas and cylinders parallel to the thermal flux

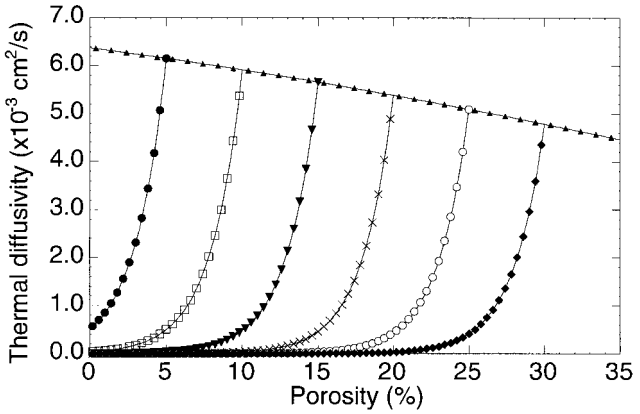

Fig. 12 Thermal diffusivity versus porosity. Each curve refers to a mixture of closed porosity (lamellas perpendicular to the thermal flux) and open porosity, for a total amount of: ●, 5%; □, 10%; ▼, 15%; ×, 20%; ○, 25%; ◆, 30%; curve.▲ is the same as in Fig. 11.

The shape of porosity can, in general, be much more critical than its percentage; a fixed porosity value was used in this study to calculate the effect on thermal diffusivity by changing the ratio between lamellar and open porosity. For a mixture of open and closed porosity (lamellas):

$$k_0 = \left[\left(\frac{4-9p}{10}\right) + \sqrt{\left(\frac{4-9p}{10}\right)^2 + \left(\frac{1-p}{5}\right)}\right](1-p_0+p)^{50}$$

$$\alpha = \frac{}{C_p\,\rho_p\,p_0 + C_0\,\rho_0\,(1-p)(1-p_0+p)}$$

(Eq 7)

where now p is the open porosity and p_0 is the total amount of porosity. C and ρ are, respectively, the specific heat and density of pores (p) and bulk matrix (0), whereas k_0 is the thermal conductivity of the bulk material. In this way, $p_0 - p$ is the lamellar porosity fraction.

The results are shown in Fig. 12, where the thermal diffusivity is reported for different values of porosity. Assuming a constant total porosity, each curve shows the change in thermal diffusivity produced by a change from 100% closed to 100% open porosity. From the calculated trends, it is clear that diffusivity is a highly nonlinear function of the lamellar porosity content.

On the basis of the analysis, a possible explanation for the observed trend of thermal diffusivity versus coating thickness (Fig. 9) can be proposed; that is, the total porosity of each sample is a mixture of open porosity and a small percentage of closed porosity (lamellas perpendicular to the thermal flux). Supposing that the closed porosity varies from about 2.5% in the thinner coatings to about 1.5% for the thicker ones, the experimentally observed increase in thermal diffusivity can be justified by the model of Fig. 12.

In this case, the total porosity increases slightly with the thickness (Fig. 7); therefore, it seems impossible to interpret the observed increase of thermal diffusivity in terms of total porosity change. In fact, even if the total porosity increases, a small reduction in the content of closed porosity can lead to an increase in diffusivity. This is possible if the variation refers to the fraction of small pores that can be present on the submicron scale (Ref 16), but are not easily detectable by microscopy.

As observed previously, the change in t-m phase composition is correlated with the diffusivity data, with the latter increasing with the m-phase content. There are no data available on the thermal diffusivity in bulk samples or single crystals of tetragonal and monoclinic Y-PSZ; therefore a direct effect of the phase transformation on the heat conduction within the ceramic cannot be excluded. However, because there is a considerable volume expansion (~4%, as can be easily calculated from the variation in cell parameters) during the t-to-m phase transformation, it is presumed that interlamellar pores tend to shrink, with an overall effect of reduction in the volume of closed porosity.

Such a hypothesis needs to be supported by a detailed experimental analysis. This viewpoint suggests the formation of the m-phase to be a negative feature that reduces the effectiveness of the thermal barrier in addition to the well-known negative effects on the mechanical stability of the coating (Ref 4).

6. Conclusions

Plasma spray deposition of Y-PSZ thermal barrier coatings under uncontrolled surface temperature conditions leads to different phase composition and thermal transport properties of the material. In this study there was a strict correlation between phase percentage of zirconia polymorphs, thermal diffusivity, and thickness of a set of APS coatings deposited on nickel-base alloy substrates without any control of the coating temperature during the process. In particular, the monoclinic phase content and the thermal diffusivity increased with the coating thickness; because these changes occurred with a slight increase in the total porosity, a clear interpretation of the results was not trivial.

A possible explanation relates the heat conduction mechanism to percentage, shape, and orientation of the porosity. It was proposed that the volume expansion associated with the t-to-m phase transformation causes a progressive reduction of the lenticular closed porosity parallel to the surface, resulting in an enhanced thermal diffusivity within the TBC.

The results discussed in this article clearly indicate the importance of the temperature control on phase equilibrium in Y-PSZ coatings, as well as on their thermal properties.

Acknowledgment

This work was partially funded by PF-MSTAII " Special Materials for Advanced Technologies," CNR—National Council of Researches.

References

1. V.P. Swaminathan and N.S. Cheruvu, Gas Turbine Hot-Section Materials and Coatings in Electric Utility Applications, *Advanced Materials and Coatings for Combustion Turbines*, V.P. Swaminathan and N.S. Cheruvu, Ed., ASM International, 1994
2. *Proc. Quadriennial International Conf. Power Stations*, 13-15 Oct 1997, Association Ingenieurs de Montflory, 1997
3. M.G. Hocking, V. Vasantaree, and P.S. Sidky, *Metallic & Ceramic Coatings: Production, High Temperature Properties & Applications*, Longman Scientific & Technical, Harlow, Essex, UK, 1989
4. P. Scardi, M. Leoni, and L. Bertamini, Residual Stress in Plasma Sprayed Partially Stabilised Zirconia TBCs: Influence of the Deposition Temperature, *Thin Solid Films*, Vol 278, 1996, p 96-103
5. L.C. Aamodt, J.W. Maclachlan Spicer, and J.C. Murphy, Analytical of Characteristic Thermal Transit Times for Time-Resolved Infrared Radiometry Studies of Multilayered Coatings, *J. Appl. Phys.*, Vol 68 (No. 12), 1990, p 6087-6098
6. D.P. Almond and P.M. Patel, *Photothermal Science and Techniques*, Chapman & Hall, London, 1996
7. L. Fabbri, F. Cernuschi, P. Fenici, S. Ghia, and G.M. Piana, Photothermal Techniques for Nondestructive Characterisation of Turbine Blade Coatings, *Materials for Advanced Power Engineering, Part II*, D. Coutsouradis et al., Ed., Kluwer Academic, Dordrecht, The Netherlands, 1994, p 1377-1381
8. G. Busse and H.G. Walther, Photothermal Nondestructive Evaluation of Materials with Thermal Waves, *Progress in Photothermal and Photoacoustic Science and Technology*, Vol 1, *Principles and Perspectives of Photothermal and Photoacoustic Phenomena*, A. Mandelis, Ed., Elsevier Science, 1992, p 218-222
9. Technical bulletin No. 10.311, Metco Inc., Westbury, NY1985
10. P. Scardi, L. Lutterotti, and P. Maistrelli, Experimental Determination of the Instrumental Broadening in the Bragg-Brentano Geometry, *Powder Diffr.*, Vol 9 (No. 3), 1994, p 180-186

11. M. Leoni and P. Scardi, A Computer Program for Structural Refinement from Thin Film XRD Patterns, *Mater. Sci. Forum*, Vol 278-281, 1998, p 177-182
12. B. Shultz, Thermal Conductivity of Porous and Highly Porous Materials, *High Temp.-High Press.*, Vol 13, 1981, p 649-660
13. D.S. McLachlan, An Equation for Conductivity of Binary Mixtures with Anisotropic Grain Structures, *J. Phys. C: Solid State Phys.*, Vol 20, 1987, p 865-877
14. A.D. Brailsford and K.G. Major, The Thermal Conductivity of Aggregates of Several Phases, Including Porous Materials, *Br. J. Appl. Phys.*, Vol 15, 1964, p 313-319
15. A. Bjorneklett, L. Haukeland, J. Wigren, and H. Kristiansen, Effective Medium Theory and the Thermal Conductivity of Plasma-Sprayed Ceramic Coatings, *J. Mater. Sci.*, Vol 29, 1994, p 4043-4050
16. R. McPherson and B.V. Shafer, Interlamellar Contact within Plasma-Sprayed Coatings, *Thin Solid Films*, Vol 97, 1982, p 201-204